

COMPARING ULTRA-HIGH TEMPERATURE OXIDATION MECHANISMS OF HAFNIUM AND HAFNIUM-CARBIDE FOR HYPERSONIC APPLICATIONS

Christopher J. Recupero, Connor J. Stephens, Elizabeth J. Opila

University of Virginia

Department of Materials Science and Engineering

Abstract

The need for materials to withstand higher temperatures in oxidizing environments is critical for hypersonic flight. This paper examines two materials that have the potential to be used in these environments: Hf and HfC. Experiments were performed on Hf and HfC in high-temperature oxygen environments to analyze the role of carbon on oxidation. A custom resistive heating system was used to perform experiments at 1600, 1700, and 1800°C for up to 11 minutes in a 1%O₂-Ar environment. It was observed that the role of carbon in HfC is to disrupt the oxide scale by forming CO(g) and creating a porous oxide structure. A thin carbon-rich oxide interlayer is also observed, although it does not appear to aid in making the oxide protective. The oxide growth in HfC was observed to follow linear kinetics, likely due to the highly porous oxide structure. Hf was observed to follow a parabolic oxidation rate prior to breakaway oxidation, as the nonporous oxide became more protective over time, up to a certain point. Breakaway oxidation for Hf is observed after a certain amount of oxide growth, when the rate of oxide growth increased, indicating that HfC may be better suited for high-temperature oxidizing environments.

Introduction

The advancement of hypersonic (Mach 5+) vehicles is largely dependent on the development of materials able to withstand the harsh environmental conditions experienced during flight. Aircraft surfaces such as wing leading edges and flight control surfaces will experience temperatures upwards of 3000°C

due to stagnation points on sharp edges and close contact with the shockwave. These sharp edges are necessary to enable maneuverability at hypersonic speeds. Current material technology uses SiC based system which are limited by relatively low melting temperatures and active oxidation. C-C based systems have melting temperatures >4000°C but actively oxidize. However, Group IV, V and VI transition metal carbides also have high melting temperatures suitable for hypersonic flight¹. HfC has been shown to have one of the highest melting temperatures at 3928°C. However, despite the high melting temperatures, these materials are known to have poor oxidation resistance and their oxidation behaviors are not well understood. The oxidation of HfC results in a porous scale structure by the following mechanisms:



Equation (1) represents the overall reaction stoichiometry and Equation (2) represents the carbide/oxide interface reaction². The CO(g) and CO₂(g) break up oxide formation and create a porous network as they diffuse through the oxide. This can increase the rate of oxidation by allowing the oxygen to penetrate rapidly through the growing oxide and continue to react more rapidly with the HfC. Barger et al.³ describe the presence of an interlayer between the HfC and the HfO₂ and identify it as an oxycarbide. Scott et al.⁴ later identify this interlayer as an oxide + carbon layer, which is more protective against oxidation because of its dense morphology. Pure Hf is less expensive

and easier to manufacture than HfC. However, despite the extensive literature on both materials, no direct comparison of metal and carbide oxidation, which shows the effect that carbon has on mechanisms or kinetics, has been made. Understanding the role of carbon on high temperature oxidation behavior is critical to better inform the design of oxidation resistant materials.

Experimental Methods

a. Custom Resistive Heating System

A resistive heating system (RHS), based on the design of Karlsdottir and Halloran⁵ and modified by Shugart and Opila⁶, and Backman and Opila⁷, was used to conduct the oxidation experiments. A schematic of the RHS is shown in Figure 1a. Samples inside the RHS are connected to Cu leads which deliver currents of over 100 A. Since the samples are shaped into the dogbone shape, as shown in Figure 1b, the

reduced cross-sectional area of the “hot zone” allows the sample to undergo Joule heating. The current running from the copper leads heats the hot zone to the desired temperature. The current is delivered by a furnace control unit equipped with a Eurotherm controller (BPAN controller, MicroPyretics Heaters International, Inc., Cincinnati, OH). The furnace controller receives temperature input from an emissivity-correcting pyrometer (Pyrofiber Lab, Pyrometer Instrument Co., Windsor, NJ) which adjusts the power output to match the desired temperature. Temperature control can be maintained up to 1800°C with an accuracy of roughly $\pm 20^\circ\text{C}$ at 1300°C and $\pm 50^\circ\text{C}$ at 1800°C. To prevent potential reaction between the HfC and the Hf samples with the copper leads, Pt foil is wrapped around the copper leads. Y-stabilized ZrO₂ (YSZ) padded alligator clips are used to ensure stable connection with the sample and the Pt-wrapped copper.

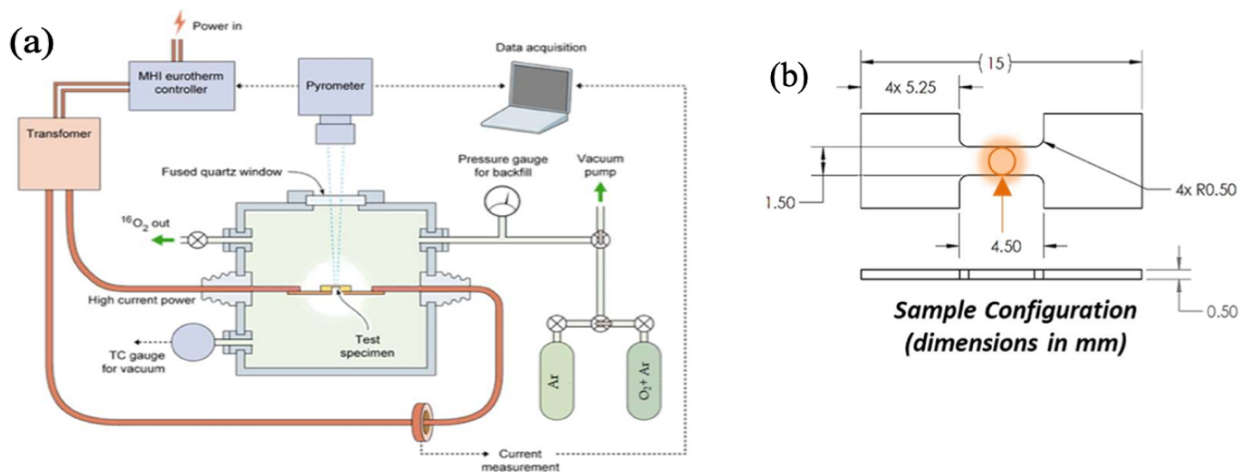


Figure 1: (a) Schematic Diagram of the RHS system at UVA and (b) the Hf and HfC samples used in this project

b. Materials

A sheet of 0.635mm (0.020 in.) thick Hf (99.5% pure, metals basis) was sectioned into RHS specimens via electrical discharge machining (EDM; Exothermics, Inc., Amherst, NH, USA). P1200 SiC foils were used to lightly ground the EDM samples to remove

residue from the machining process. Three-inch HfC pucks produced by hot isostatic pressing (HIP; Kurt J. Lesker Company, Pittsburgh, PA) were diamond machined (Bomas Machining Specialties, Inc., Woburn, MA) into the dogbone geometry of 0.5mm (0.020 in.) thick. Instrumental gas analysis

(IGA) was performed (Evans Analytical Group, Syracuse, NY) to verify the carbon content of the unoxidized HfC. This confirmed a carbon content of 49.6 at% C (6.2 wt% C), correlating to HfC_{0.992}.

c. Oxidation Experiments

Samples were loaded into the RHS, and alligator clips were used to clip the samples to the conductive leads. The chamber was evacuated and backfilled with Ar until the pressure reached 50 mTorr or lower. Pure Ar was then introduced into the chamber until the chamber was at atmospheric pressure. Once at pressure, a gas exit valve was opened so that Ar flowed continuously through the chamber. Gas flow was maintained at 950-1000 sccm for the duration of each experiment. HfC samples were heated to the desired temperature at 1.5°C/s in the pure Ar flow. Due to the delicate nature of the HfC samples, intermittent dwell times were also incorporated into the ramping procedure to prevent samples from cracking during temperature ramp. The Hf was heated at a rate of 5°C/s. Once the sample was at a stable temperature, the gas was switched to a flowing 1% O₂-Ar mixture (1000 sccm). Oxidation time started when oxygen was introduced to the system, and current flow was stopped at the end time of the experiment. The experimental setup with the sample at elevated temperature is shown in Figure 2.

When the current was stopped, the sample cooled to near room temperature in only a few seconds. Oxidation experiments were conducted at 1600°C, 1700°C, and 1800°C for HfC and were run up to 11 minutes. The high reflectivity of Hf would at times cause errors in the pyrometer readings, preventing accurate temperature measurement of the material. Therefore, oxidation of Hf was limited to the temperature of 1600°C. Experiments were conducted for 2 min, 5 min, 7 min, and 10 min.

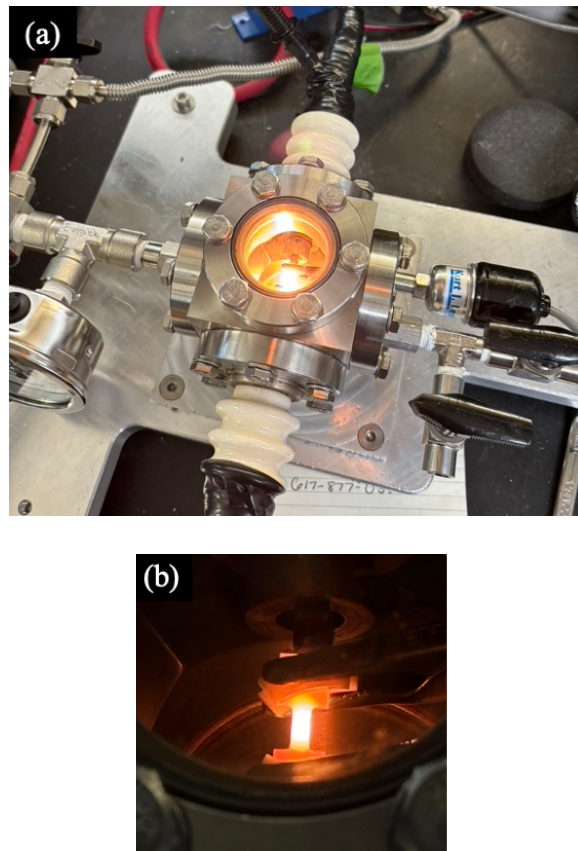


Figure 2: The experimental set-up (a) with HfC sample at elevated temperature (b).

d. Sample preparation and Imaging

Once the samples were removed from the RHS chamber, they were broken in half. Samples were then mounted in epoxy, polished, sputter-coated, and analyzed using scanning electron microscopy (SEM). Foils of HfC were prepared using focused ion beam milling (FIB) and investigated via transmission emission microscopy (TEM). A diagram of the sectioned sample is shown in Figure 3.

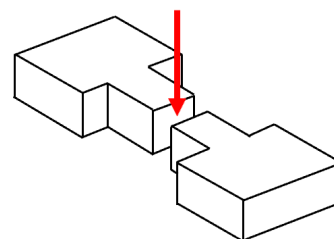


Figure 3: Diagram showing the method of cross-section for the samples.

Results and Discussion

Backscattered electron SEM micrographs of Hf samples exposed to oxygen at 1600°C for 2, 5 and 7 min are shown in Figure 5. Very little oxide growth occurs at less than 2 min for Hf as shown in Figure 4a. In Figure 5, slight HfO_2 growth at the corner of the 2 min oxygen exposed Hf sample is visible. Oxide growth starts at the corners followed by the short sides, and then the long sides. The long sides are less affected by edge effects and are thus more representative of bulk Hf. Therefore, kinetic data was gathered from the long sides of the Hf samples. Oxidation kinetics were measured via recession of the bulk material.

After greater exposure time, oxide grown on Hf formed one of two microstructures: a highly cracked oxide or a two-phase layer of $\alpha\text{-Hf}+\text{HfO}_2$. If the cracked oxide microstructure formed, the oxide is commonly non-adherent to the Hf bulk. In this microstructure, long needles in the two-phase structure are observed. If the other microstructure formed, when the HfO_2 remained adherent to the Hf, a two-phase region existed between the solid Hf and HfO_2 . This two-phase transition layer contains the $\alpha\text{-Hf}$ and HfO_2 in a finger-like microstructure in a radial distribution around the underlying Hf. The factors influencing whether the microstructure develops as a cracked, non-adherent, needle-like structure or as a two-phase $\alpha\text{-Hf} + \text{HfO}_2$ finger-like structure are not fully understood and warrant further investigation in future work. Micrographs of these two different oxide formations at higher magnification are shown in Figure 6.

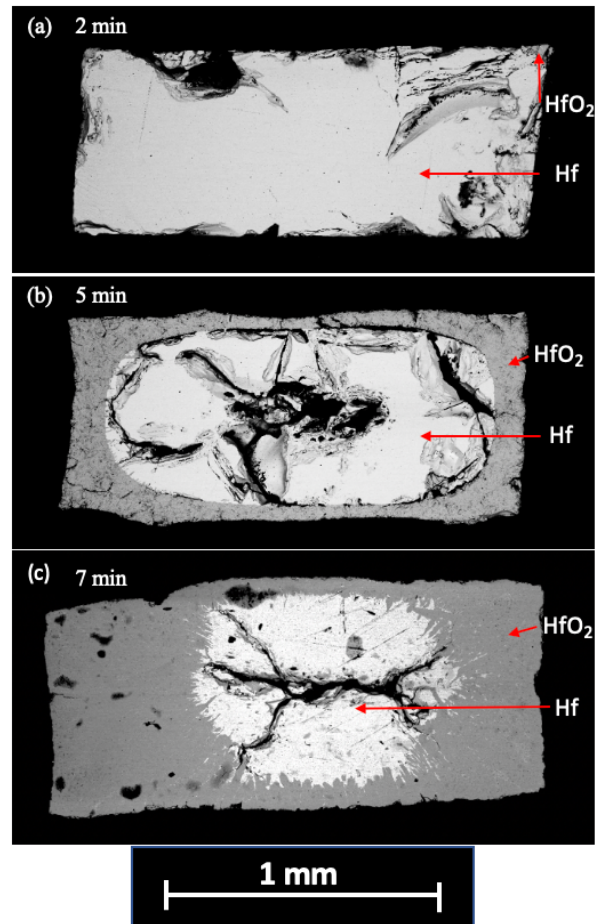


Figure 4: Hf samples oxidized in 1% O_2/Ar at 1600°C for 2 min (a), 5 min (b) and 7 min (c). The oxide growth is observed.

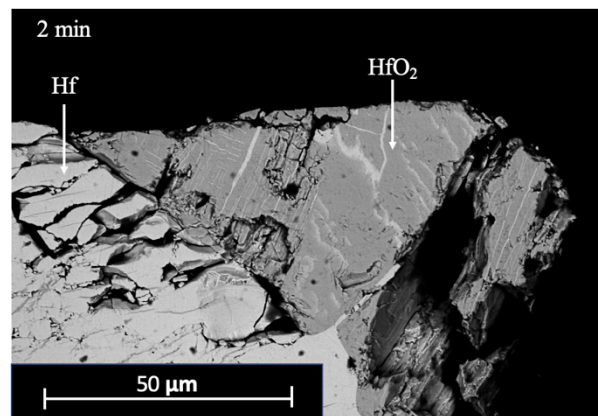


Figure 5: Formation of oxide on the corner of the Hf sample exposed for 2 min. in 1% O_2/Ar at 1600°C.

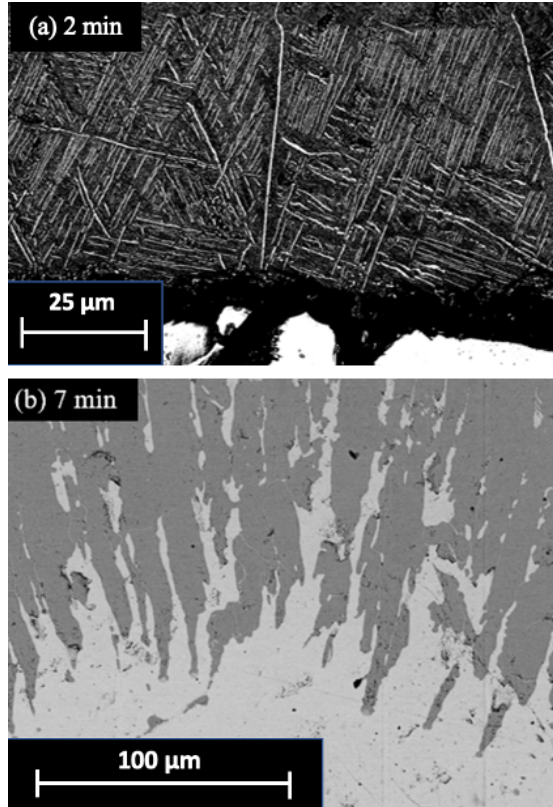


Figure 6: Backscattered electron SEM micrographs for Hf samples after oxidation at 1600°C in 1%O₂-Ar. (a) The Hf sample is exposed to oxygen for 5 min and the non-adherent needle-like oxide microstructure is observed. (b) The Hf sample is exposed to oxygen for 7 min and the adherent finger-like microstructure is observed.

Sometimes, bulging of the oxide on Hf is observed, visible in Figure 4c. This bulging effect is more noticeable after longer oxygen exposures. The Pilling Bedworth Ratio (PBR) describes the ratio of the molar volume of the oxide to the molar volume of the substrate. Hf has a PBR calculated to be 1.59. The HfO₂ phase grown on the surface of the Hf is in compression, as it is constrained by the smaller size of the Hf metal bulk. As it grows, the HfO₂ in the middle is compressed more and pushes out into free space, forming the bulging structure observed. A schematic of this phenomenon is drawn in Figure 7

Unlike Hf, the oxidation of HfC forms a Maltese cross, as depicted in Figure 8. This is evident for all conditions studied for this project.

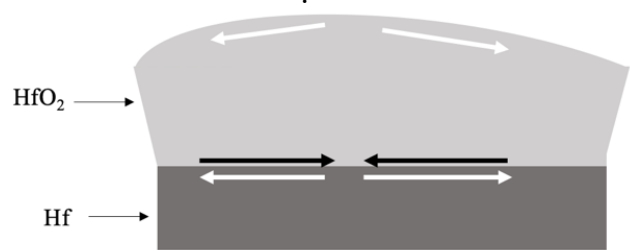


Figure 7: Schematic of Hf oxide growth, initially being constrained in compression by the smaller Hf compound and then stretching in tension away from the surface as the oxide grows in free space.

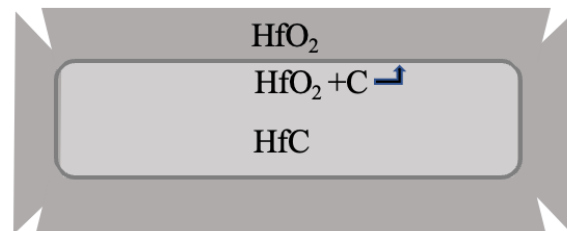


Figure 8: Maltese cross formation during HfC oxidation

In Figure 9, it is observed that longer oxygen exposure times at the same temperature of 1600°C allowed for oxide to grow. These oxygen exposure times were designated at 2, 5 and 7 minutes. Two distinct oxide layers are visible at each oxygen exposure time and a porous oxide scale is observed.

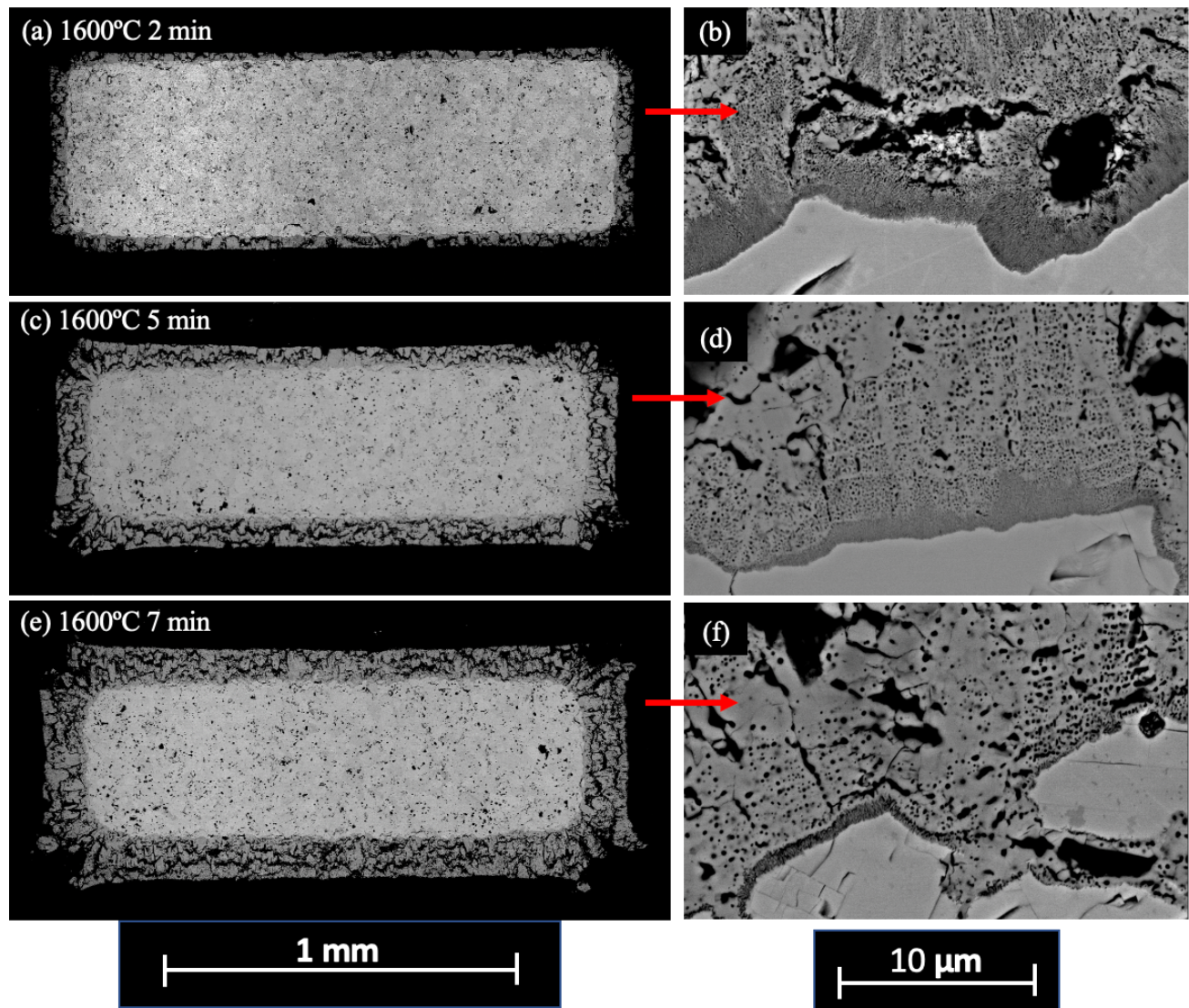


Figure 9: Backscattered electron SEM micrographs taken on HfC samples oxidized at 1600°C for 2 minutes (a,b), 1600°C for 5 minutes (c,d), 1600°C for 7 minutes (e,f), all in 1%O₂-Ar. Oxide growth is observed for increasing time, and at higher magnification, the microstructure is observed to be similar for all three durations. Two distinct oxide layers are observed for each sample.

In Figure 10, micrographs of HfC after 5 minute exposures in 1%O₂-Ar at 1600, 1700, and 1800°C are shown. The same Maltese cross formation is observed for all three

temperatures. Additionally, two distinct oxide layers are observed. Grain boundary oxidation is evident for all three temperatures, particularly on the sample oxidized at 1800°C.

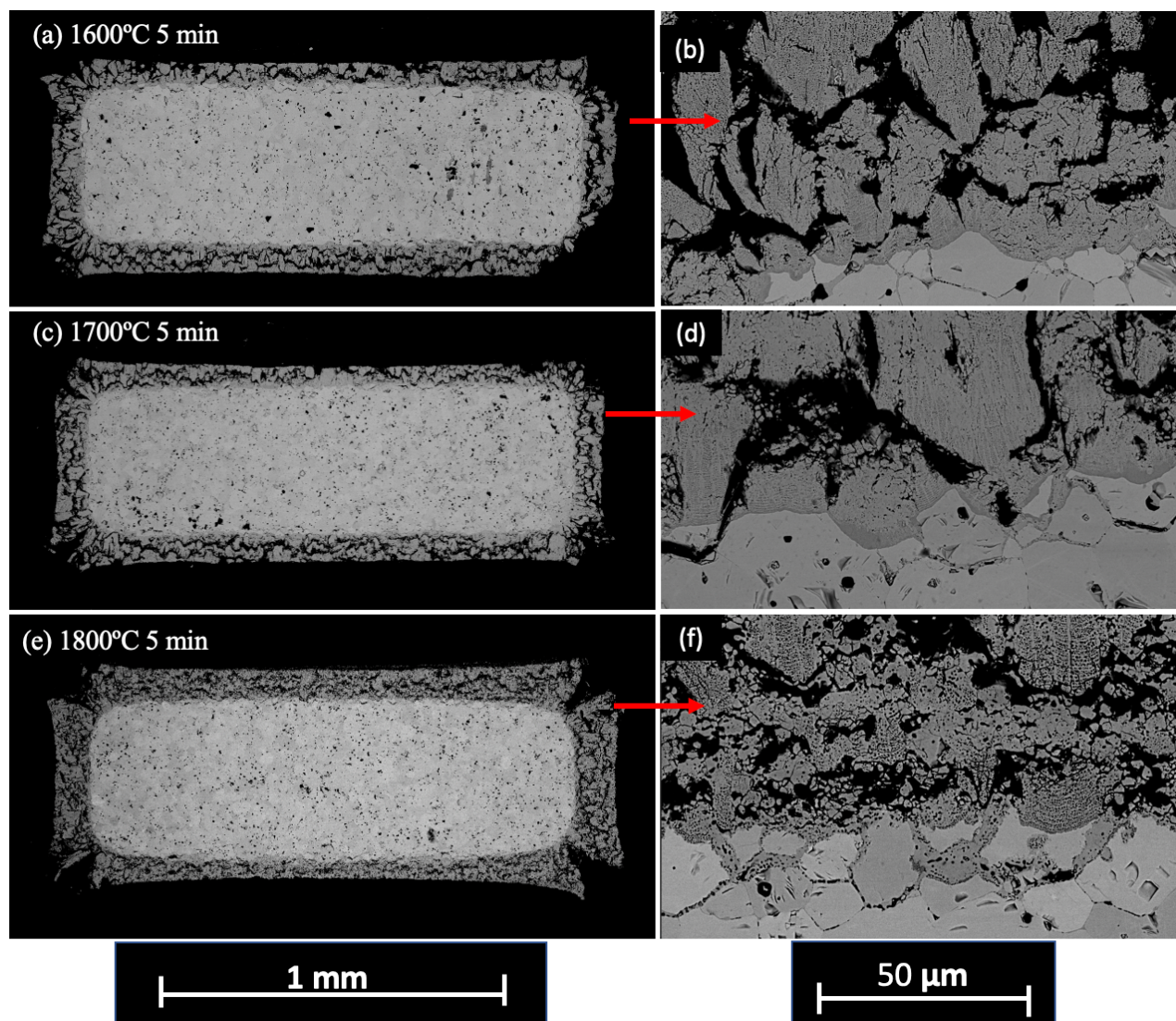


Figure 10: Backscattered electron SEM micrographs of HfC after oxidation in 1%O₂-Ar at 1600°C for 5 minutes (a,b), 1700°C for 5 minutes (c,d) and 1800°C for 5 minutes (e,f). The Maltese cross formation is observed along with a similar oxide structure for all three temperatures.

Further investigation of the composition of the oxide layers was performed using EDS and TEM. Figure 12 shows the EDS line scan performed across the boundary from the HfC bulk to the oxide. The observed interlayer was confirmed to be a carbon rich interlayer. TEM analysis was then performed and the results in Figure 11 show this carbon-rich interlayer with

carbon distributed in a finger-like morphology in this interlayer. The interlayer takes the form of phase separated HfO₂+ C. The form of these carbon deposits is discussed in literature⁴ although, the thicknesses of this interlayer is observed to be much thinner in these experiments compared to literature.

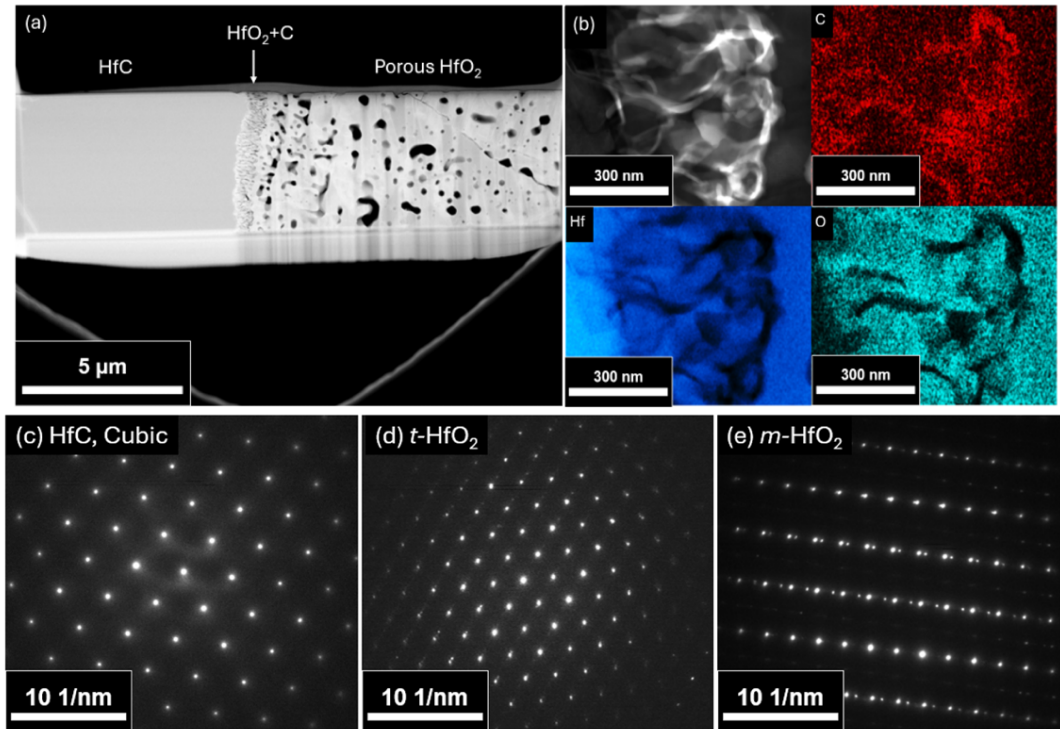


Figure 11: (a) TEM micrograph of a FIB liftout from oxidized HfC across the carbide/inner/outer layer boundaries; (b) TEM/EDS of the HfO₂+C layer; and (c-e) SAED patterns from the areas around the inner layer, showing (c) cubic HfC below the oxide, (d) tetragonal HfO₂ in the HfO₂+C layer, and (e) monoclinic HfO₂ in the bulk oxide. HfC oxidized at 1600°C for 7min in 1%O₂-Ar.

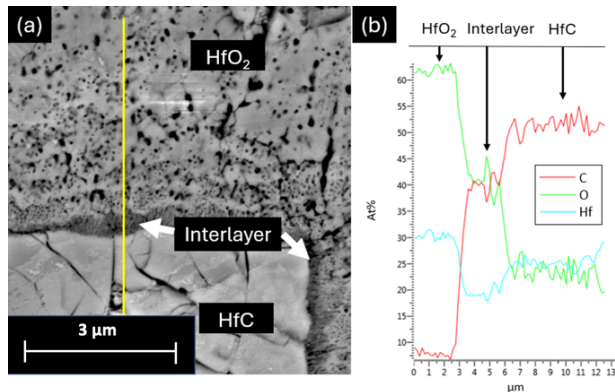


Figure 12: (a) Backscatter cross section SEM micrographs of HfC post-oxidation across the carbide/oxide boundary and (b) an EDS line scan across the interlayer. HfC oxidized at 1600°C for 5min in 1%O₂-Ar

The formation of this interlayer can be explained by the hypothesis which is visualized in Figure 14. As the HfC is initially exposed to

oxygen, single phase oxide begins to grow on the surface of the HfC. In this initial phase (shown in steps 2 and 3), it is proposed that the surface of the HfC bulk has enough exposure to the oxygen, so there is no carbon-rich HfO₂ +C oxide interlayer. Because the carbon-rich interlayer was observed in all conditions, this phase occurs prior to 2min of oxidation time. As the oxide grows, the oxygen partial pressure at the HfC/oxide interface decreases. A certain point is reached when the partial pressure becomes too low to oxidize the carbon into CO or CO₂, at which point the carbon-rich layer forms. Over time, the oxygen partial pressure increases at this substrate/oxide interface such that the carbon deposits in this layer are oxidized and CO(g) forms, leaving behind the layers of pores observed in the HfO₂.

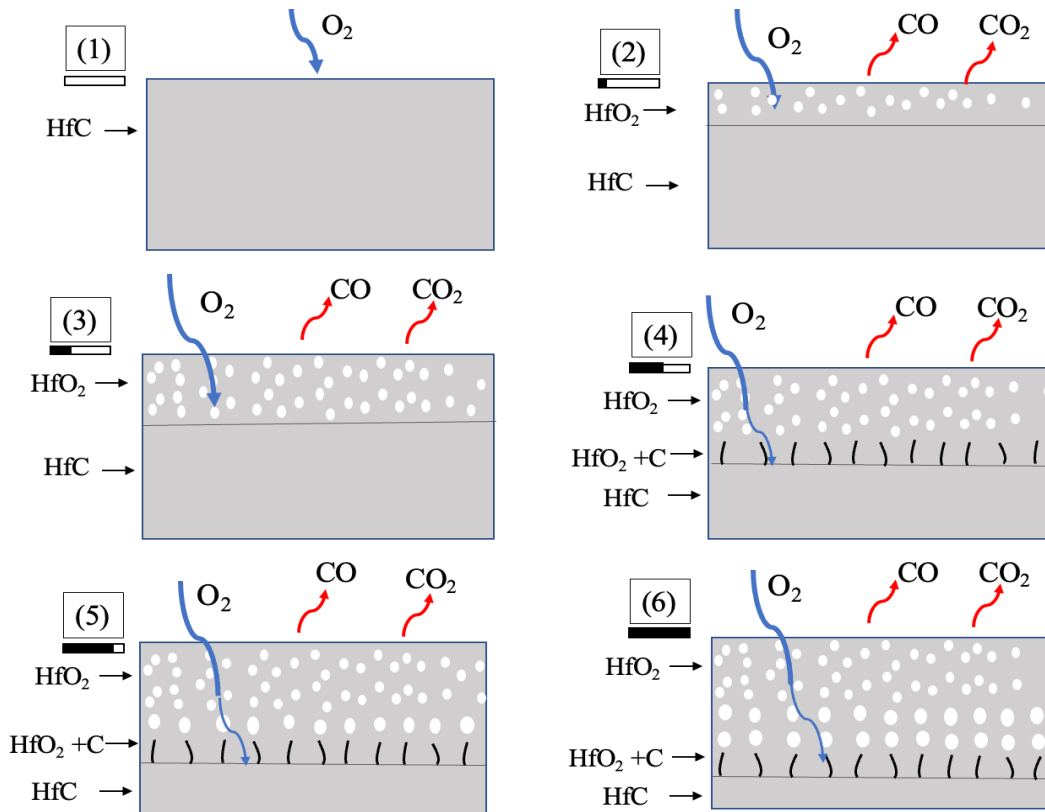


Figure 13: The process of HfC oxidation growth over time. The progress bars follow the time progression. Initially, the oxygen partial pressure is high enough, so the carbon oxidizes into CO and subsequently CO₂. After a certain amount of oxidation growth, the oxygen pressure becomes low enough that the carbon-rich layer forms. This carbon-rich interlayer continues to oxidize over time to form the porous layered structure.

Recession data was analyzed to compare Hf and HfC oxidation rates as shown in Figure 14. It is evident that the Hf grows in thickness at short oxygen exposure times, as the oxygen diffuses into the bulk. Sometime between 2 minutes and 5 minutes of oxygen exposure, oxide growth expands beyond the corners and short sides, and it grows on the long sides, representative of the bulk material. It was observed that Hf recession more closely followed a parabolic rate, indicating that solid state diffusion is occurring through the dense oxide, up until the breakaway oxidation point. The recession is negative because the interstitial oxygen dissolved into the Hf metal, swelling the bulk material. The non-porous oxide phase, unlike the porous oxide observed on HfC, protects the Hf metal from increased oxidation growth. However, after 7 minutes,

breakaway oxidation occurred, likely due to the tensile forces shown in Figure 7, causing cracks to form and provide a fast path for oxygen ingress. The Hf oxidized for 10 minutes was shown to exhibit a considerably higher recession depth.

The HfC recession kinetics are shown to more closely follow a linear rate in Figure 15, indicating that gas diffusion of the oxygen is occurring through large cracks and voids in the oxide. Additionally, the differences between recession rates for the different temperatures studied are not shown to be statistically significant. Breakaway oxidation is not observed for HfC, with similar oxidation rates observed at all experimental temperatures. This absence of breakaway oxidation when compared to the breakaway oxidation observed in Hf may be explained by the porous oxide

morphology. HfC is calculated to have a PBR of 1.45, lower than the 1.59 PBR for Hf. This lower PBR for HfC and the porous oxide structure diminishes the tensile forces experienced by the larger oxide phase compared to the HfC bulk, perhaps preventing breakaway oxidation in HfC. The porous oxide in HfC yields a linear rate as seen in Figure 15c.

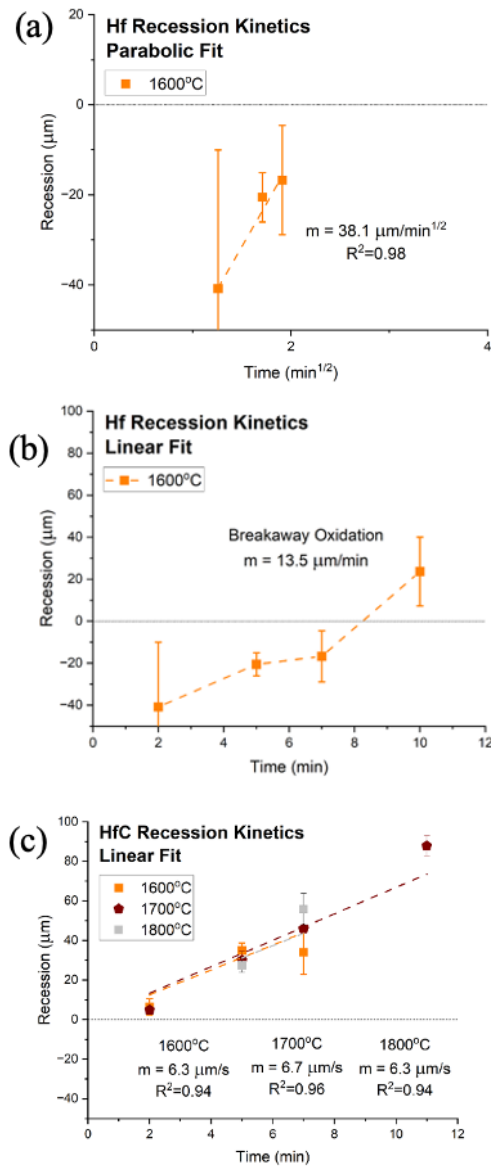


Figure 15: Recession Kinetics for Hf (a,b) at 1600°C and HfC (c) at 1600, 1700, 1800°C

Conclusions

High temperature oxidation experiments were conducted for Hf and HfC in temperatures ranging from 1600°C to 1800°C for durations ranging from 2 to 11 minutes. It was observed that Hf followed a parabolic oxide growth rate until a breakaway oxidation point when the material recession rate greatly increased. This parabolic rate behavior indicated the oxygen travels via solid state diffusion through the dense oxide. This breakaway oxidization may be explained by the bulging oxidation growth behavior and loss of protective capability due to the high PBR. HfC was observed to form a more porous oxide due to the formation of gaseous CO. The HfC recession was observed to follow linear oxidation kinetics indicating that the oxygen travels via gas-phase diffusion through large cracks and voids, and the carbon-rich oxide interlayer did not act as a barrier to oxidation growth. The porous oxide scale and the Maltese cross oxide growth released growth stresses in HfC, preventing the breakaway oxidation experienced in the Hf.

References

- [1] E. Wuchina, E. J. Opila, M. Opeka, W. Fahrenholtz, and I. G. Talmy (2007).
- [2] Courtright, E.L., Prater, J.T., Holcomb, G.R. *et al. Oxidation of Metals* **36**, 423–437 (1991).
- [3] Bargeron, C. B., Benson, R. C., Jette, A. N. & Phillips, T. E. *J. Amer. Ceram. Soc.* **76**, 1040–1046 (1993).
- [4] Scott, J. A., He, X. & Lipke, D. W. *J. Amer. Ceram. Soc.* (2022) doi:10.1111/jace.18941.
- [5] Karlsdottir, S. N. & Halloran, J. W. *J. Amer. Ceram. Soc.* **90**, 3233–3238 (2007).
- [6] Shugart, K and Opila, E. *J. Am. Ceram. Soc.*, vol. **98**, no. 5, pp. 1673–1683 (2015)
- [7] Backman, L., Graham, K., Dion, M., & Opila, E. *High Temperature Corrosion of Materials* (2024)